International Journal of Nanomedicine

Dovepress
open access to scientific and medical research

Open Access Full Text Article

ORIGINAL RESEARCH

Antibacterial and osteogenesis performances of LL37-loaded titania nanopores in vitro and in vivo

This article was published in the following Dove Press journal:
International Journal of Nanomedicine

Xinkun Shen[1]
Mohammed A Al-Baadani[1]
Hongli He[1]
Lina Cai[1]
Zuosu Wu[1]
Litao Yao[1]
Xinghai Wu[1]
Shuyi Wu[1]
Mengyu Chen[1]
Hualin Zhang[2,3]
Jinsong Liu[1]

[1]School and Hospital of Stomatology, Wenzhou Medical University, Wenzhou 325027, People's Republic of China; [2]College of Stomatology, Ningxia Medical University, Yinchuan 750004, People's Republic of China; [3]General Hospital of Ningxia Medical University, Yinchuan 750004, People's Republic of China

Background: Many studies have shown that the size of nanotube (NT) can significantly affect the behavior of osteoblasts on titanium-based materials. But the weak bonding strength between NT and substrate greatly limits their application.

Purpose: The objective of this study was to compare the stability of NT and nanopore (NP) coatings, and further prepare antibacterial titanium-based materials by loading LL37 peptide in NP structures.

Methods: The adhesion strength of NT and NP layers was investigated using a scratch tester. The proliferation and differentiation of MC3T3-E1 cells on different substrates were evaluated in vitro by CCK8, alkaline phosphatase activity, mineralization and polymerase chain reaction assays. The antibacterial rates of NP and NP/LL37 were also measured by spread plate method. Moreover, the osteogenesis around NP and NP/LL373 in vivo was further evaluated using uninfected and infected models.

Results: Scratch test proved that the NP layers had stronger bonding strength with the substrates due to their continuous pore structures and thicker pipe walls than the independent NT structures. In vitro, cell results showed that MC3T3-E1 cells on NP substrates had better early adhesion, spreading and osteogenic differentiation than those of NT group. In addition, based on the drug reservoir characteristics of porous materials, the NP substrates were also used to load antibacterial LL37 peptide. After loading LL37, the antibacterial and osteogenic induction abilities of NP were further improved, thus significantly promoting osteogenesis in both uninfected and infected models.

Conclusion: We determined that the NP layers had stronger bonding strength than NT structures, and the corresponding NP materials might be more suitable than NT for preparing drug-device combined titanium implants for bone injury treatment.

Keywords: titanium, nanotubes, nanopores, LL37 peptide, antibacterial, osteogenesis

Introduction

As common orthopedic and dental materials, titanium and its alloys have excellent mechanical properties and biocompatibility.[1] However, their bio-inert surfaces greatly limit the early osseointegration capacities.[2] Surface nano-topological treatment has been proved to be an effective way to improve the biocompatibility of titanium.[3–5] Some nanostructures can effectively interact with the adsorbed proteins or cell receptors, thus affecting the behavior of adherent cells.[6] In the existing nanostructures, titania nanotubes (NTs) have attracted wide attention due to their regular tubular nanostructures and size controllability.[7,8] It had been proved that small NTs could significantly increase the early adhesion and proliferation of osteoblasts/mesenchymal stem cells, while large NTs could greatly promote the

Correspondence: Hualin Zhang
804# Shengli South Street, Xingqing District, Yinchuan City, Ningxia Province, People's Republic of China
Tel +860 951 674 3450
Email hua31415926@163.com

Jinsong Liu
268# Xueyuan West Road, Lucheng District, Wenzhou City, Zhejiang Province, People's Republic of China
Tel +8 605 778 806 6085
Email jinsong0719@wmu.edu.cn

submit your manuscript | www.dovepress.com
DovePress
http://doi.org/10.2147/IJN.S198583

osteogenic differentiation and antioxidant capacities.[9–12] Through comprehensive comparison in vitro and in vivo, it has been determined that the most suitable size for promoting bone formation is about 70 nm.[10,12]

Recent study has shown that the length, size and morphology of NTs can effectively affect the adsorption of functional proteins.[13] Therefore, other properties of NTs besides size may also affect the behavior of subsequent adhesion cells, which is rarely discussed in previous studies. Although NTs have remarkable osteogenic abilities, the weak bonding between NT layers and substrates greatly limits their clinical application.[14] Some studies indicate that regular nanopore (NP) structures can be obtained instead of NTs by regulating electrolyte composition, electrolytic voltage or time.[15,16] These NP samples have continuous pore-like structures and thick partition walls. In my analysis, the continuous pores may bring stronger stability to NP layers. Meanwhile, the thick walls may provide more attachment sites for cells, thus promoting cell adhesion and other behaviors. Therefore, through a preliminary understanding of the structural differences, we made the assumption that NP might have the better stability and bone-promoting properties than NT substrates under the same pipe diameter.

In addition to the inertia of titanium-based implants, bacterial infection is also considered to be one of the major factors hindering osseointegration.[17–19] The infection rates in revision total knee and hip arthroplasty are around 4.57% and 1.94%, respectively.[19] Staphylococcus aureus (*S. aureus*) and drug-resistant *S. aureus* (such as MRSA: Methicillin-resistant *S. aureus*) are regarded as the most common bacteria causing orthopedic infections. Once the invading bacteria (only 100 bacteria per gram of tissue) adhere to implant surface, they quickly proliferate and form a dense film, thus hindering the bactericidal effects of subsequent antibacterial drugs.[20] Therefore, it is necessary to prepare titanium implants with excellent early antibacterial properties through drug-instrument combination. In previous researches, NT samples have been used as the carriers for loading some antibacterial drugs (eg, antibiotics, antibacterial peptides, metal ions, etc.).[21–23] Because of the similar tubular structures, we believe that NP substrates can also be used to prepare antibacterial implants via loading antimicrobials.

As a common cationic antimicrobial peptide, LL37 has been demonstrated to have excellent bactericidal activity and does not cause bacterial resistance.[24,25] Researches show that almost all cells can release LL37 peptide in vivo. The broad-spectrum antibacterial property of LL37 is mainly due to its ability to destroy bacterial membrane.[26] In addition to its antibacterial properties, LL37 has also been shown to participate in the process of immune regulation and stem cell recruitment.[27–29] Thus, LL37 peptide was chosen to be loaded by NP substrates for constructing antibacterial and pro-osteogenesis implant. In this work, the following three issues will be addressed: 1) to prepare NT and NP structures on Ti surface, and compare their stability and biological properties; 2) to construct LL37-loaded NP samples (NP/LL37), and evaluate their antibacterial and osteogenic induction functions in vitro (Scheme 1); 3) to further verify the osteogenesis around NP/LL37 implants using both non-infected and infected models in vivo.

Materials and methods

Materials

Ti foils (purity: 99.6%; thickness: 1 mm; diameter: 10 mm) and wires (diameter: 1 mm; length: 1 mm) were purchased from Advent Research Materials Ltd. (Oxford, UK). Ammonium fluoride was provided by Kangpuhuiwei Technology Co., Ltd. (Beijing, People's Republic of China). Ethylene glycol was obtained from Aladdin Industrial Co. (Shanghai, People's Republic of China). LL37 peptide (LLGDFFRKSKEKIGKEFKRIVQRIKDF LRNLVPRTES, 98%) was purchased from Jier Biotechnology Co. (Shanghai, People's Republic of China). Bicinchoninic acid (BCA) and p-nitrophenyl phosphate assay kits were provided by Beyotime Biotechnology Co., Ltd. (Jiangsu, People's Republic of China).

Samples preparation and characterization

Ti foils and wires were first polished with gradient sandpapers (No. 600–1500), and then cleaned with ethanol, acetone and distilled water under ultrasonic condition (300 W, 40 KHz, each for 15 mins). Next, cleaned Ti samples and platinum foil were used as the anode and cathode for anodic oxidation treatment, respectively. The distance between the two electrodes was about 3 cm. For the preparation of NT structures, glycerol electrolyte containing 0.51 wt% NH_4F and 8.1 wt% H_2O was employed. Samples were first oxidized for 3 hrs at 20 V, and then treated with high voltage oxidation (170 V, 2 mins) and ultrasonic (5 mins) to remove these NT layers. The above samples were further oxidized at 20 V for 20 mins to obtain the final NT substrate. For the preparation of NP samples, a procedure similar to NT was carried out. However, ethylene glycol electrolyte containing 0.38 wt% NH_4F and 1.8 wt% H_2O was employed, and the reaction voltage was 50 V instead of 20 V.

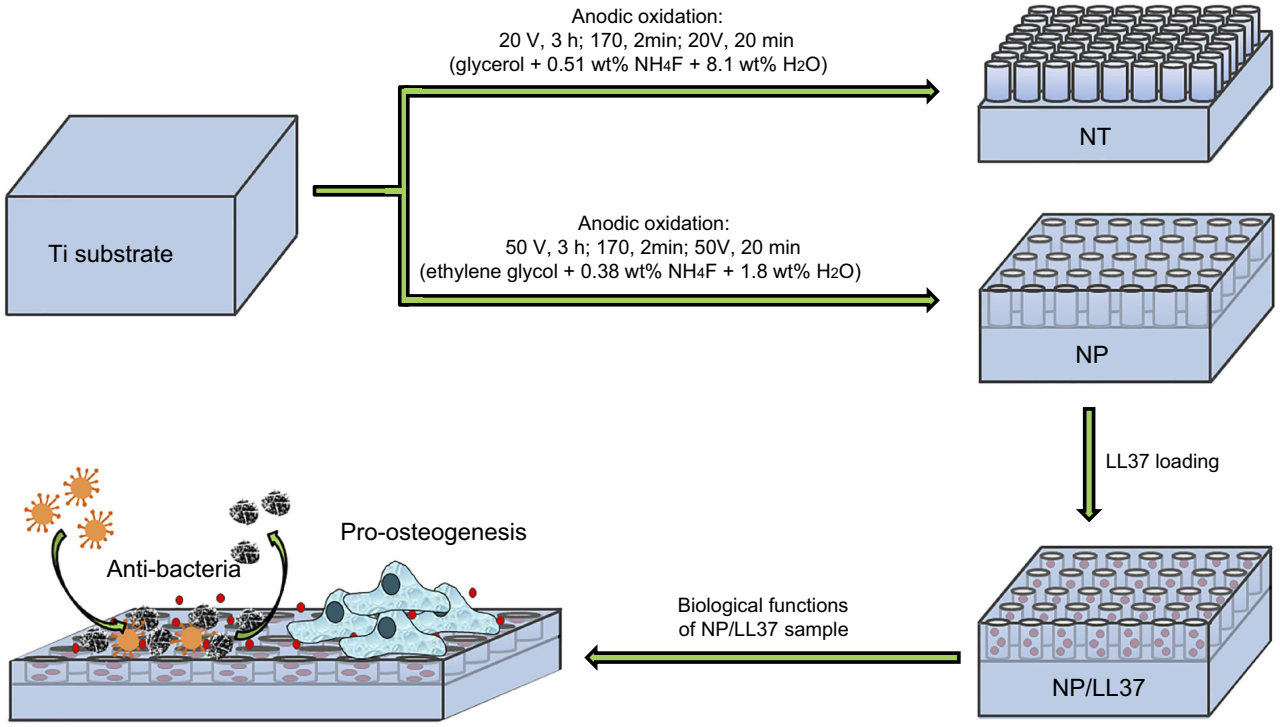

Scheme 1 Schematic illustration of the preparation processes and/or biological functions of different substrates.

To prepare LL37-loaded NP samples (NP/LL37), 5 mg of LL37 peptide was first dissolved in distilled water (1 mL) and stored at −20°C. Next, 10 μL of LL37 solution (5 mg/mL) was evenly spread on the surface of NP substrates, and further loaded by simplified lyophilization method (vacuum drying at ambient temperature for 30 min).[22,30] The final NP/LL37 samples were obtained after 20 repetitions.

Surface morphology and roughness were characterized by scanning electron microscopy (SEM; JSM-6700F, JEOL, Tokyo, Japan) and atomic force microscopy (AFM; Dimension, Bruker, Germany), respectively. Surface crystalline phase and water contact angle were measured by X-ray diffraction (D/Max 2500PC, Rigaku, Japan) and a video-based optical system (Model 200, Future Scientific, Taiwan, People's Republic of China), respectively. Adhesion strength at the interfaces of NT/NP layers and Ti substrates was investigated via the scratch test (progressive load: from 1 to 10 N) using a scratch tester (CSM Instruments, Switzerland).

LL37 release

Two substrates in each group were immersed into 10 mL of PBS solution (pH 7.4). After incubation for different time (4, 12, 24, 48, 72, 120 and 168 hrs) under constant shaking (25 rpm) at 37°C, 0.3 mL of release solution was collected and measured with a commercial BCA phosphate kit. New PBS solution (0.3 mL) needed to be replenished after each sampling to keep the total volume of solution at 10 mL. In order to determine the total amount of LL37 loaded by NP/LL37, two specimens were soaked into 2% SDS solution under ultrasonic condition (300 W, 40 KHz) for 2 hrsl. After centrifugation for 5 mins (12,000 rpm), LL37 in the supernatant was detected with BCA phosphate kit.

Osteoblast assays

Osteoblast adhesion and morphology

MC3T3-E1 cells were obtained from Shanghai Institute of Cell Biology, and cultured with α-MEM medium supplemented with 10% FBS at 37°C under 5% CO_2 atmosphere. The initial seeding density of MC3T3-E1 cells was around 1×10^4cells/cm^2. For adhesion assay, cells were seeded onto NT and NP substrates for 0.5 and 2 hrs. The adherent cells were then stained by H33258 solution and observed with a CLSM (TCS SP5, Leica, Germany). For exploring cell morphology, MC3T3-E1 cells on NT and NP substrates were fixed with paraformaldehyde (4%) and stained by rhodamine-phalloidin and H33258 after culturing for 2 d. Finally, cells were observed using an inverted fluorescence microscope (FM, OLYMPUS IX71, Japan).

Osteoblast viability

MC3T3-E1 cells on Ti, NT, NP or NP/LL37 substrates were cultured for different time (1, 3 and/or 7 d). Then, mixture solution of DMEM medium (180 μL) and CCK8 solution (20 μL) was added to each well, incubated for another 4 hrs, and finally measured at 450 nm with a spectrophotometric microplate reader (Bio-Rad 680, USA).

Alkaline phosphatase (ALP) activity

MC3T3-E1 cells on Ti, NT, NP or NP/LL37 substrates were cultured for 7 d with osteogenic differentiation medium (α-MEM medium supplemented with 10 mM β - glycerophosphate sodium, 0.05 mM vitamin C and 100 mM dexamethasone). Then, cells were lysed by 1% Triton X-100 at 4°C for 40 min. ALP activity and total proteins in lysate were measured with the p-nitrophenyl phosphate and BCA kits at 490 and 570 nm, respectively.

Mineralization

After culturing MC3T3-E1 cells for 7 and 14 d with osteogenic differentiation medium, paraformaldehyde (4%) and alizarin red solution (pH 4.1) were used to fix and stain the adherent cells, respectively. These stained cells were then treated by acetic acid (10% v/v) and ammonium hydroxide (10% v/v), and quantitatively measured at 405 nm with a spectrophotometric microplate reader (Bio-Rad 680, USA).

Expression of osteogenic genes

After culturing MC3T3-E1 cells for 7 d with osteogenic differentiation medium, the expression of ALP, collagen Ⅰ (COL Ⅰ), osteocalcin (OCN) and osteoprotegerin genes was detected with the related primers (Table 1), and normalized by GAPDH gene. The cDNA obtained by reverse transcription was amplified using a Bio-Rad CFX Manager system under 95°C for 3 mins, followed by 40 cycles of 95°C for 5 s and 60°C for 30 s.

Table 1 Real-time polymerase chain reaction primers used in this study

Target genes	Primers
ALP	F: 5′- GAACAGAACTGATGTGGAATACGAA - 3′
COL Ⅰ	R:5′- CAGTGCGGTTCCAGACATAGTG - 3′
OCN	F: 5′- GATGTTGAACTTGTTGTTGCTGAGGG - 3′
OPG	R: 5′- GGCAGGCGAGATGGCTTATT - 3′
	F: 5′- GAACAGACAAGTCCCACACAGC - 3′
	R: 5′- TCAGCAGAGTGAGCAGAAAGAT - 3′
	F:5′- ATTGGCTGAGTGTTTTGGTGGA - 3′
	R:5′- GCTGGAAGGTTTGCTCTTGTGA - 3′
GAPDH	F:5′- CTCGTCCCGTAGACAAAATGGT - 3′
	R:5′- GAGGTCAATGAAGGGGTCGTT - 3′

Antibacterial rates

S. aureus (ATCC6538) and MRSA (ATCC1761) were cultured onto NP and NP/LL37 substrates at an initial density of 1×10^6 cells/cm^2. After culturing for 12 hrs in MHB medium at 37°C, the adherent and free bacteria were, respectively, collected with 3 mL PBS via a violent shock. The diluted bacteria were then seeded onto sterile agar plates for 12 hrs, and counted to calculate the bacterial concentrations.

Osteogenesis assessment in vivo

Twenty male rats (about 380–450 g) were provided by Wenzhou Medical University and used for animal experiments with their approval of Animal Ethics Committee. All animal assays were strictly performed according to the guidelines of the Institutional Animal Care and Use Committee. Rats were randomly divided into normal (non-infected) and infected groups (10 rats in each group). NP (20 implants) and NP/LL37 (20 implants) were used to investigate the osteogenesis in vivo in this study. Two implants of each group were inserted into rat femur (one implant per hind leg). In bacterial model, 100 μL of *S. aureus* (1×10^7 cells/mL) were carefully injected into implantation holes before inserting different implants.

After implantation for 8 weeks, all rats were killed to investigate the new bone formation around different implants (within 0.5 mm) via micro-computed tomography analysis. The specific analysis area was about 1 mm below the epiphyseal line. Data were analyzed with the algorithms of three-dimensional finite element (SCAN VivaCT40 V6.1 software).

Statistical analysis

All data were expressed as means±SD. The statistical analysis was performed with OriginPro (version 7.5) via Student's Two-Sample *t*-test and one-way ANOVA. The confidence levels were set as 95% (*$p<0.05$).

Results and discussion

Surface characterization of NT and NP

The SEM images and related statistics showed that pore size of NT and NP was around 72.8±8.7 and 77.6±6.5 nm, respectively (Figure 1A and B). Length of NT and NP was also similar and about 2.7±0.3 and 2.6±0.4 μm (Figure 1A and D). Unlike to the size and length results, the wall thickness of NT and NP was significantly different

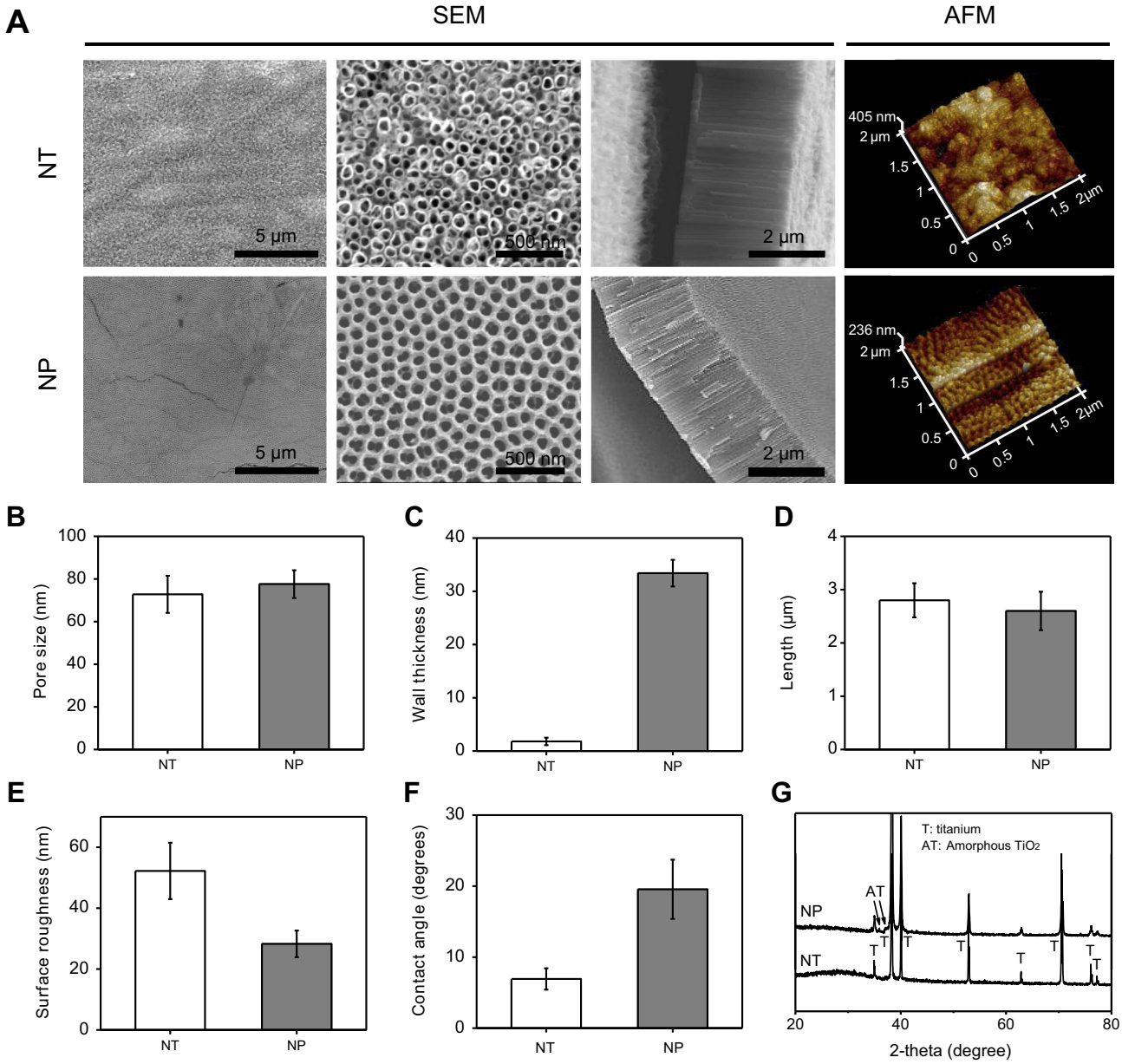

Figure 1 **(A)** Scanning electron microscopy (SEM) and atomic force microscopy (AFM) images of NT and NP substrates; statistics of pore size **(B)**, wall thickness **(C)** and length **(D)** of surface nanotubes and nanopores; **(E)** statistics of surface roughness according to AFM images; **(F)** water contact angle and **(G)** X-ray diffraction (XRD) patterns of NT and NP substrates.

(Figure 1A and C). Independent tubular structures (wall thickness around 1.8±0.7 nm) were observed on NT surface. However, NP surface presented a continuous pore-like structure, and the wall thickness was around 33.4±2.5 nm. The difference in morphology and wall thickness might be attributed to the different electrolytic voltage and electrolyte composition.[14,15] Schmuki et al claimed that water content in electrolytes was a key factor to affect the formation of oxide tubes or pores, and NP structures were easier to emerge in a low water environment.[14] Sulka et al further proved that pore size could be obviously changed by changing the applied voltage (from 30 to 60 V).[15] Moreover, AFM results displayed that the surface roughness (Ra) of NT and NP was around 52.3±9.3 and 26.2±4.4 nm, respectively (Figure 1A and E).

Next, compared to that of NT group (~6.9±1.5°), water contact angle of NP samples was slightly higher and about 19.4±4.2° (Figure 1F). Because increasing the surface roughness of hydrophilic materials would reduce their apparent contact angles, the above wettability change might be due to the decrease of NP roughness.[31,32] Moreover, previous studies had proved that the biological

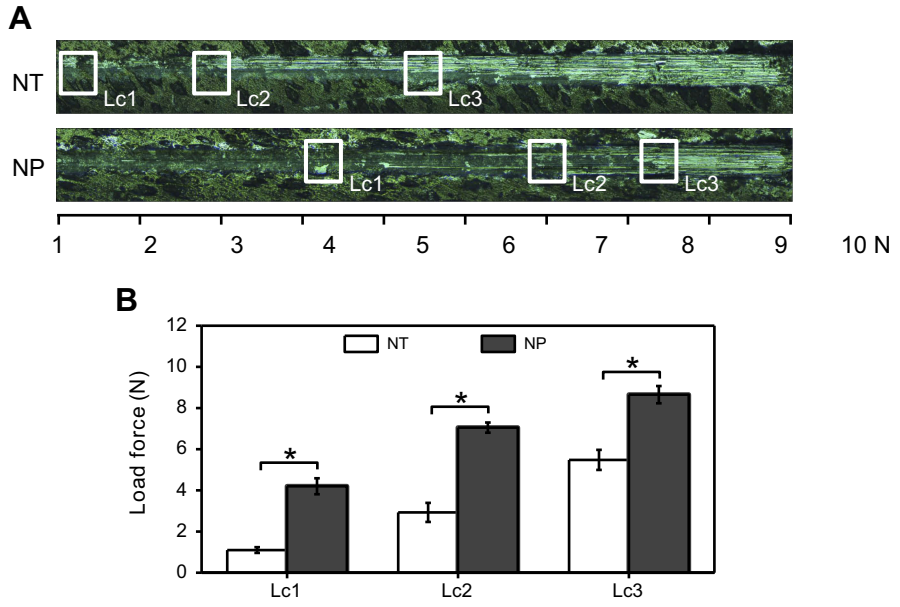

Figure 2 (**A**) Representative scratch track image of NT and NP; (**B**) statistics of critical loads of cohesion (Lc1), adhesion (Lc2) and breakthrough (Lc3). Error bars represent mean±SD for n=4, *p<0.05.

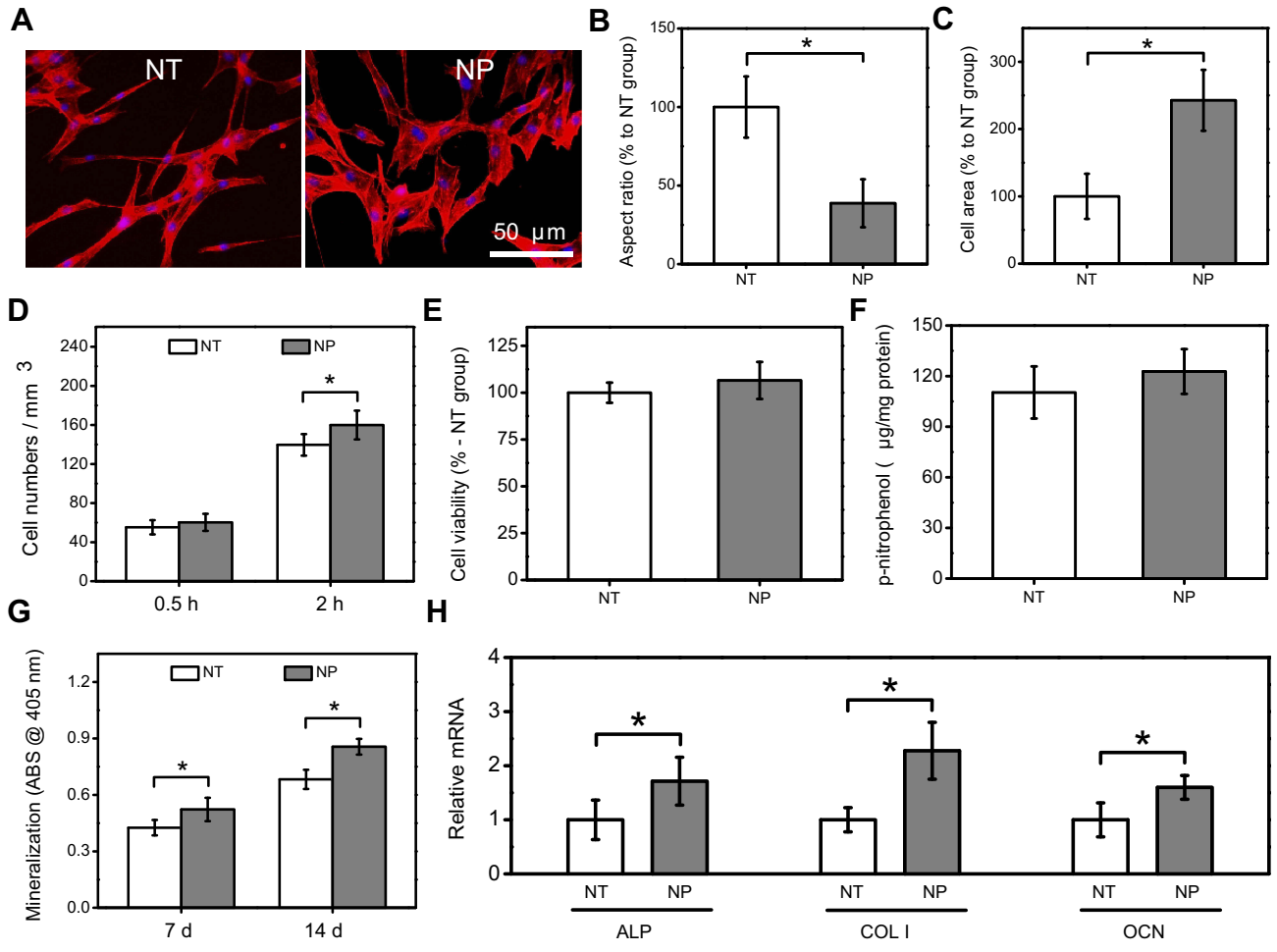

Figure 3 (**A**) Morphology of MC3T3-E1 cells on NT and NP substrates; statistics of cell aspect ratio (**B**) and area (**C**) according to morphology images; (**D**) early adhesion of MC3T3-E1 cells at 0.5 and 2 hrs; (**E**) cell viability, (**F**) ALP activity, (**G**) mineralization level and (**H**) osteogenic genes expression of MC3T3-E1 cells at 7 and/or 14 d. Error bars represent mean±SD for n=6, *p<0.05.

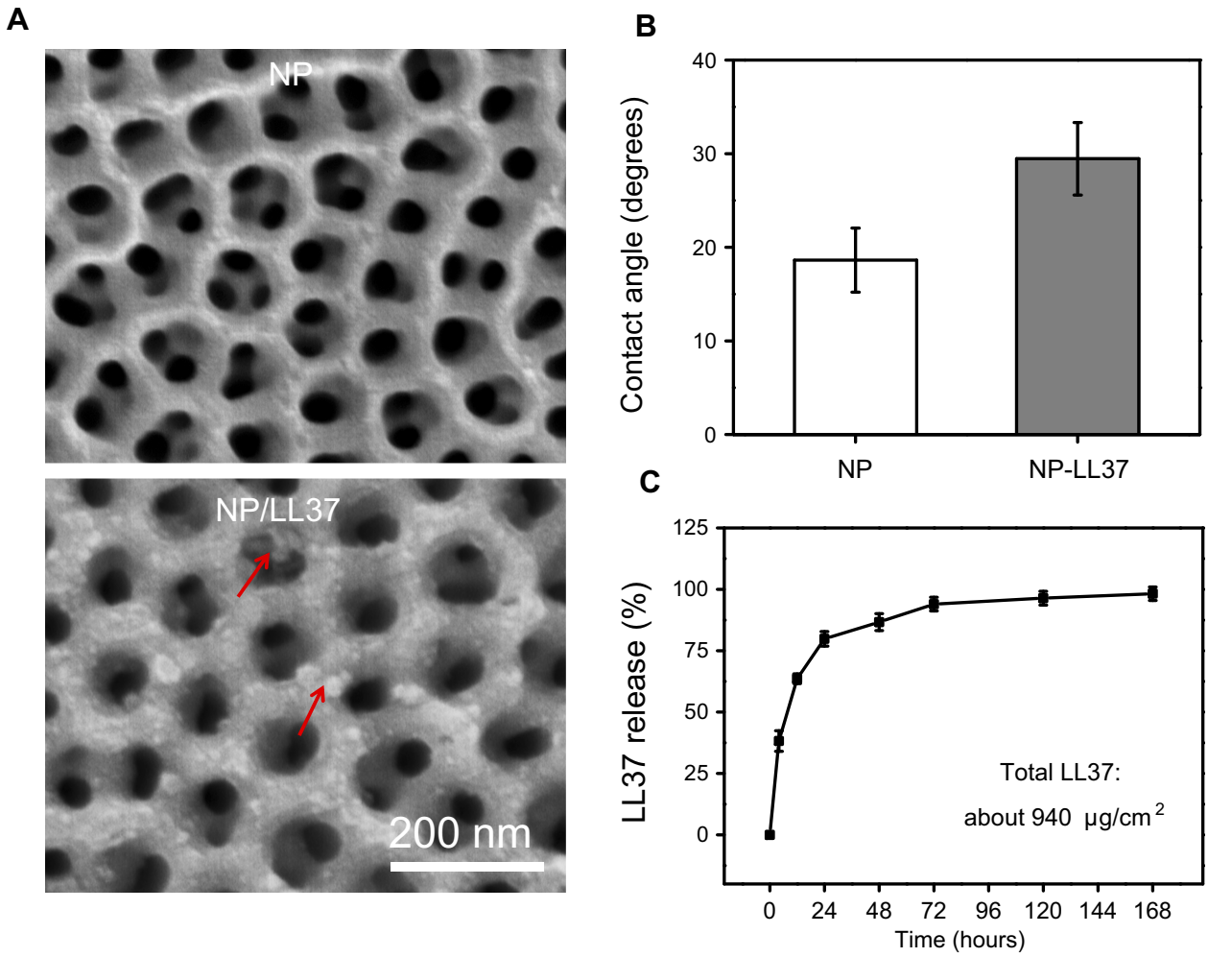

Figure 4 (**A**) Scanning electron microscopy (SEM) images and **(B)** water contact angle of NP and NP/LL37 substrates; **(C)** release profile of LL37 from NP/LL37 sample at different time. Error bars represent mean ± SD for n = 6.

behaviors of protein adhesion and cell spreading/proliferation/differentiation on material surface displayed a parabolic trend with the increase of contact angle, and the optimal wettability was about 30–55°.[33–35] Therefore, the higher contact angle of NP might be beneficial to osteogenesis induction. From the XRD patterns (Figure 1G), no significant difference was observed between NT and NP groups. Only peaks of titanium and amorphous TiO_2 were detected in this work.[11] Thus, changes in surface morphology, roughness and wettability might be involved in the regulation of adhesion, proliferation and differentiation of MC3T3-E1 cells.

Bonding strength

To investigate the stability of NT and NP layers, scratch tests were carried out.[14] The results (Figure 2) showed that the critical loads (Lc1, Lc2 and Lc3) of NT were about 1.1 ±0.1, 2.9±0.4 and 5.5±0.5 N, respectively. The Lc1, Lc2 and Lc3 of NP were 4.2±0.4, 7.1±0.3 and 8.7±0.4 N, which were 3.8, 2.5 and 1.6 times of NT group. Therefore, the bonding strength between NP coating and Ti substrate is higher, making NP structure more suitable for preparing topological Ti implants.

Comparison of cellular behaviors between NT and NP groups

As shown in Figure 3A, it was found that the morphology of MC3T3-E1 cells on NT substrates was slender, while relatively spreading in NP group.[36] Further statistics also proved that cells on NP samples had larger area and lower aspect ratio than those of NT group (Figure 3B and C). Previous studies had indicated that compared to native Ti or small nanotubes (<30 nm), large nanotubes (>70 nm) had fewer cell adhesion sites, resulting in slender cell morphology.[37,38] Therefore, the difference in cell

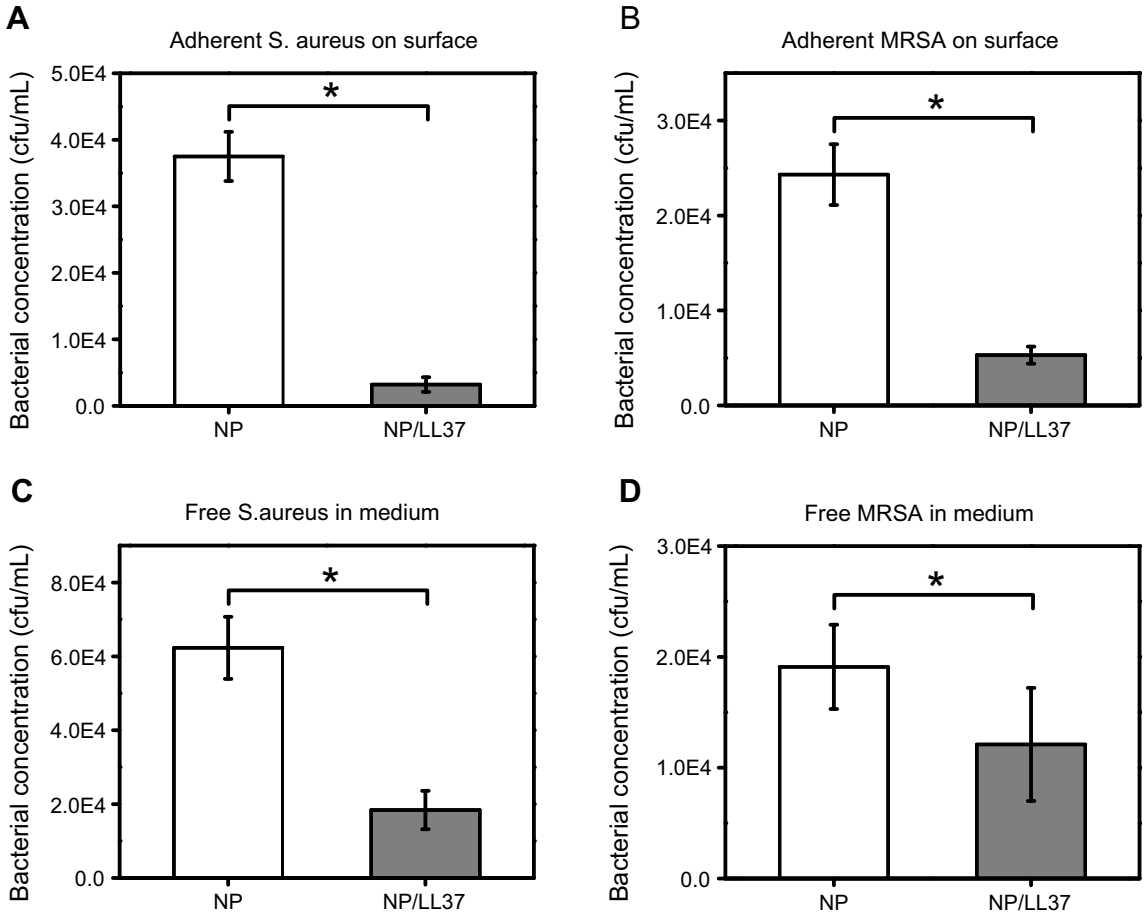

Figure 5 (**A**) Bacterial concentrations of Staphylococcus aureus (S. aureus, **A** and **C**) and Methicillin-resistant Staphylococcus aureus (MRSA, **B** and **D**) on different substrates (**A** and **B**) or in medium (**C** and **D**) at 24 h. Error bars represent mean ± SD for n = 6, *p < 0.05.

morphology was most likely due to the changes of wall thickness between NT and NP. Thick pore walls might provide more attachment sites for osteoblasts in NP group.

Another finding was that more MC3T3-E1 cells ($p<0.05$) were adsorbed onto NP surface after incubation for 2 hrs rather than 0.5 hr (Figure 3D). NP substrates also significantly ($p<0.05$) improved the mineralization level (7 and 14 d) and osteogenic genes (ALP, COL Ⅰ and OCN) expression (7 d) of MC3T3-E1 cells when comparing with NT samples (Figure 3G and H). Moreover, although the cell viability and ALP activity in NP group also slightly increased at 7 d, there was no significant difference between NP and NT groups (Figure 3E and F). The above results suggest that NP had greater potential to increase early adhesion and osteoblastic differentiation of MC3T3-E1 cells than NT structures.

NP/LL37 characterization and LL37 release

After loading LL37 peptide, some obvious sediment (red arrows) was observed on NP/LL37 surface (Figure 4A). The result of water contact angle (Figure 4B) revealed that surface of NP/LL37 was more hydrophilic (about 29.5±3.9°) than that of NP (about 18.8 ±3.4°).[39] Both results of SEM and water contact angle proved that LL37 was successfully loaded on NP surface.

Statistical analysis showed that about 940 μg/cm^2 of LL37 was successfully loaded on each NP/LL37 specimen. Since drug loading took 20 cycles, a small amount of LL37 might be lost during loading. By further calculating the theoretical value of total LL37 (~1,000 μg/cm^2) after 20 loading cycles, it could be determined that the drug loading efficiency was about 94%. From the release result (Figure 4C), we found that more than 95% of LL37 was released within 72 hrs. LL37 had a quick release in the first 24 hrs, but a slower release in the following time. Moreover, a burst release (about 40%) was obviously observed within 4 hrs, which might be due to the accumulation of many LL37 at the orifice.[40] The rapid release of LL37 could ensure that NP/LL37 had a superior antibacterial property at the initial stage of implantation.

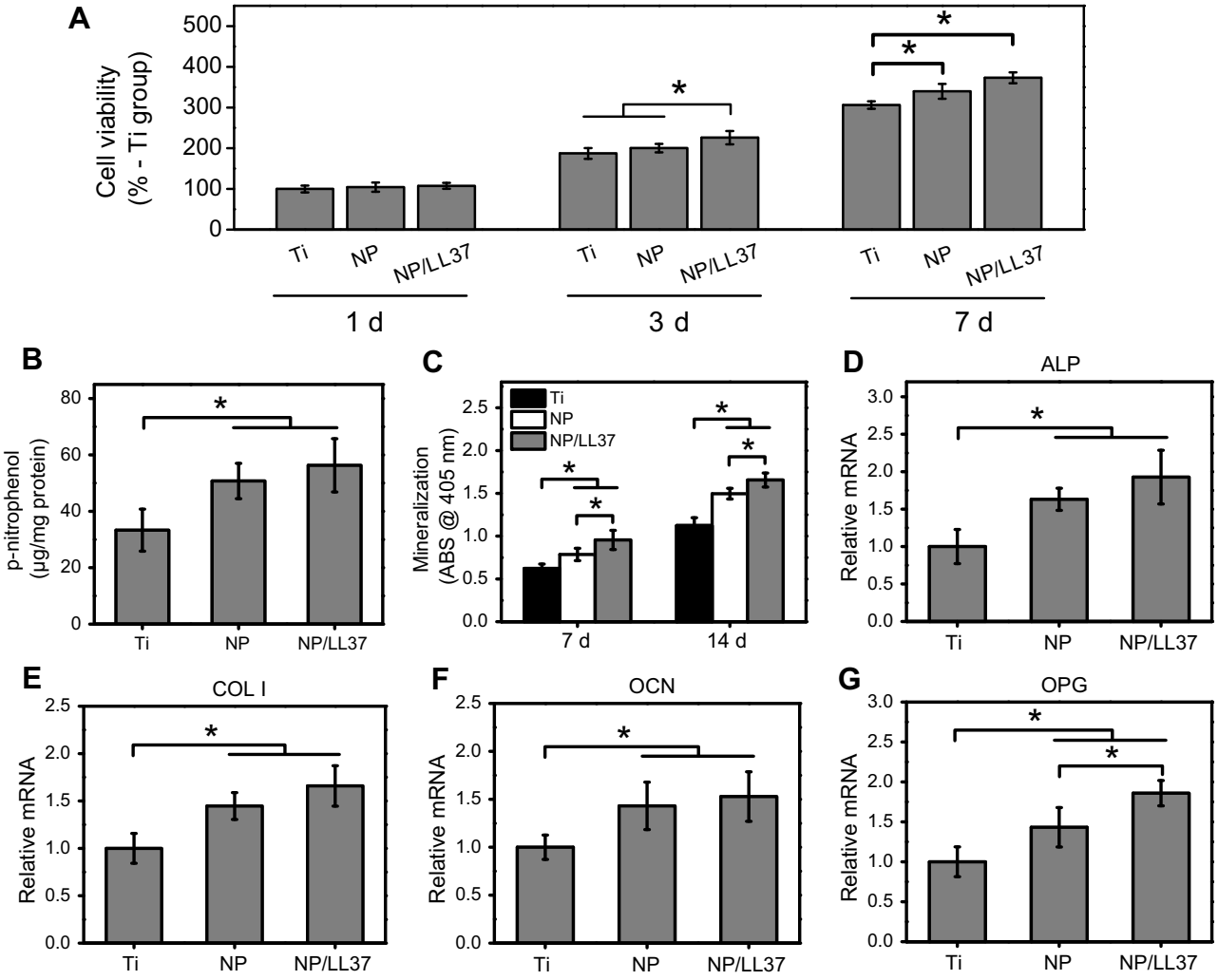

Figure 6 (**A**) Cell viability of MC3T3-E1 cells on Ti, NP and NP/LL37 substrates at 1, 3 and 7 d; (**B**) ALP activity and (**C**) mineralization level of MC3T3-E1 cells at 7 and/or 14 d; gene expression of ALP (**D**), COL Ⅰ (**E**), OCN (**F**) and OPG (**G**) at 7 d. Error bars represent mean±SD for n=6, *p<0.05.

Antibacterial property of NP/LL37 substrate

LL37 peptide has been proved to own broad-spectrum antibacterial properties in previous studies. Its antibacterial pathway can be summarized into the following three modes: carpet model, barrel stave model and toroidal pore model.[41–44] In this study, statistical analysis showed that the concentrations of *S. aureus* on NP and NP/LL37 surface were about 3.7×10^4 and 0.3×10^4 cfu/mL, and their concentrations in corresponding medium were 6.2×10^4 and 1.8×10^4 cfu/mL (Figure 5A and C). The final MRSA concentrations were also shown in Figure 5B and D, which were about 2.4×10^4 (on NP surface), 0.5×10^4 (on NP/LL37 surface), 1.9×10^4 (in NP medium) and 1.2×10^4 cfu/mL (in NP/LL37 medium), respectively. The above data indicate that NP/LL37 had excellent bactericidal properties to both bacteria (especially *S. aureus*).

Cellular behaviors of MC3T3-E1 cells on NP/LL37 substrate

There was no significant difference in cell viability at 1 d among Ti, NP and NP/LL37 groups (Figure 6A). However, the viability of MC3T3 cells on Ti, NP and NP/LL37 substrates increased successively after culturing for both 3 and 7 d (Ti < NP < NP/LL37) (p<0.05). Compared to those of Ti group, NP and NP/LL37 (especially NP/LL37) also significantly (p<0.05) improved the ALP activity (7 d), mineralization level (7 and 14 d) and some osteogenic genes expression (7 d) of MC3T3-E1 cells (Figure 6B–G). These results suggest that the loaded

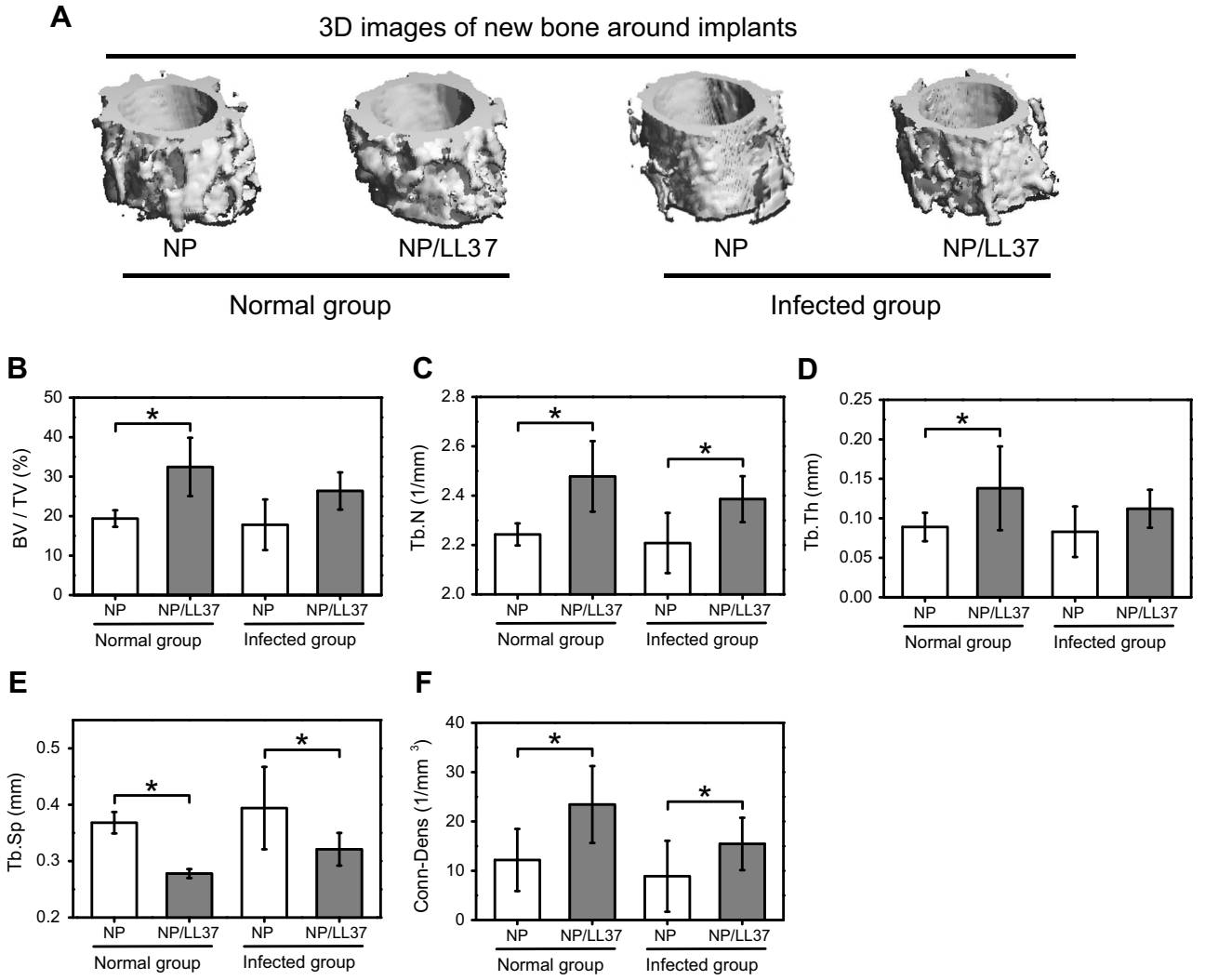

Figure 7 (**A**) 3D images of new bone in normal and infected NP and NP/LL37 groups after implantation for 8 weeks; statistics of bone volume fraction (BV/TV) (**B**), trabecular number (Tb.N) (**C**), trabecular thickness (Tb.Th) (**D**), trabecular separation (Tb.Sp) (**E**) and connectivity density (Conn-Dens) (**F**). Error bars represent mean ± SD for n = 8, *p < 0.05.

LL37 peptide could further promote cell proliferation and differentiation of MC3T3-E1 cells.[45,46]

Osteogenesis in vivo

After implantation for 8 weeks, more new bone was observed around NP/LL37 implants than NP in both normal (uninfected) and infected groups (Figure 7A). Meanwhile, after bacterial infection, the new bone mass around the two implants decreased to different degrees. Further statistic results displayed that there were similar trends in BV/TV, Tb.N, Tb.Th and Conn-Dens (Figure 7B–D and F), while an opposite trend in Tb.Sp (Figure 7E). In the normal group, the BV/TV (%), Tb.N (1/mm), Tb.Th (mm), Tb.Sp (mm) and Conn-Dens (1/mm^3) of new bone around NP implant were about 19.4±2.1, 2.24 ±0.05, 0.09±0.02, 0.37±0.02 and 12.2±6.3, which correspondingly changed to 32.5±7.4, 2.48±0.14, 0.14±0.05, 0.28±0.01 and 23.4±7.8 in NP/LL37 group. Their statistical values were also obtained in the infected groups of NP (17.8±6.4, 2.21 ±0.12, 0.08±0.03, 0.39±0.07 and 8.9±7.2) and NP/LL37 (26.4±4.7, 2.39±0.09, 0.11±0.02, 0.32±0.03 and 15.4±5.3), respectively. All results suggest that NP/LL37 greatly increased osteogenesis in both uninfected and infected animals.

Conclusion

Compared with nanotubes, continuous NP structures had stronger bonding strength with native Ti substrates, and significantly increased the early adhesion and osteoblastic differentiation of MC3T3-E1 cells. Furthermore, these NP samples had great potential to load antibacterial LL37 peptide and achieve their sustained release within 7 d. The results of cell and animal experiments further proved that LL37-loaded NP

substrates (NP/LL37) had great bactericidal and bone-promoting capacities in vitro and in vivo. All results indicate that NP-mediated materials might have excellent clinical prospects than NT-related implants.

Acknowledgments

This work was financially supported by National Natural Science Foundation of China (81870810 and 31700827), Zhejiang Provincial Science and Technology Project for Public Welfare (2015C33139) and China Postdoctoral Science Foundation funded project (2018T110946).

Disclosure

The authors report no conflicts of interest in this work.

References

1. Mishnaevsky L Jr, Levashov E, Valiev RZ, et al. Nanostructured titanium-based materials for medical implants: modeling and development. *Mater Sci Eng R*. 2014;81:1. doi:10.1016/j.mser.2014.04.002
2. Wang C, Wang S, Yang Y, et al. Bioinspired, biocompatible and peptide-decorated silk fibroin coatings for enhanced osteogenesis of bioinert implant. *J Biomat SCI Polym E*. 2018;29:1. doi:10.1080/09205063.2018.1477316
3. Jo YK, Choi BH, Kim CS, Cha HJ. Diatom-inspired silica nanostructure coatings with controllable microroughness using an engineered mussel protein glue to accelerate bone growth on titanium-based implants. *Adv Mater*. 2017;29:1704906. doi:10.1002/adma.201700681
4. Lu J, Zhang Y, Huo W, Zhang W, Zhao Y. Electrochemical corrosion characteristics and biocompatibility of nanostructured titanium for implants. *Appl Surf Sci*. 2018;434:63. doi:10.1016/j.apsusc.2017.10.168
5. Hou PJ, Ou KL, Wang CC, et al. Hybrid micro/nanostructural surface offering improved stress distribution and enhanced osseointegration properties of the biomedical titanium implant. *J Mech Behav Biomed Mater*. 2018;79:173. doi:10.1016/j.jmbbm.2017.11.042
6. Gittens RA, McLachlan T, Olivares-Navarrete R, et al. The effects of combined micron-/submicron-scale surface roughness and nanoscale features on cell proliferation and differentiation. *Biomaterials*. 2011;32:3395. doi:10.1016/j.biomaterials.2011.01.029
7. Oh S, Brammer KS, Li YS, et al. Stem cell fate dictated solely by altered nanotube dimension. *Proc Natl Acad Sci U S A*. 2009;106:2130e–e2135. doi:10.1073/pnas.0813200106
8. Song R, Zhang Y, Huang Q, et al. Facile construction of structural gradient of TiO_2 nanotube arrays on medical titanium for high throughput evaluation of biocompatibility and antibacterial property. *ACS Appl Bio Mater*. 2018;1:1056. doi:10.1021/acsabm.8b00288
9. Minagar S, Li Y, Berndt CC, Wen C. The influence of titania–zirconia–zirconium titanate nanotube characteristics on osteoblast cell adhesion. *Acta Biomater*. 2015;12:281. doi:10.1016/j.actbio.2014.10.037
10. Wang N, Li H, Lü W, et al. Effects of TiO_2 nanotubes with different diameters on gene expression and osseointegration of implants in minipigs. *Biomaterials*. 2011;32:6900. doi:10.1016/j.biomaterials.2011.06.023
11. Yu Y, Shen X, Luo Z, et al. Osteogenesis potential of different titania nanotubes in oxidative stress microenvironment. *Biomaterials*. 2018;167:44. doi:10.1016/j.biomaterials.2018.03.024
12. Lv L, Liu Y, Zhang P, et al. The nanoscale geometry of TiO_2 nanotubes influences the osteogenic differentiation of human adipose-derived stem cells by modulating H3K4 trimethylation. *Biomaterials*. 2015;39:193. doi:10.1016/j.biomaterials.2014.11.002
13. Kulkarni M, Mazare A, Park J, et al. Protein interactions with layers of TiO_2 nanotube and nanopore arrays: morphology and surface charge influence. *Acta Biomater*. 2016;45:357. doi:10.1016/j.actbio.2016.08.050
14. Yu D, Zhu X, Xu Z, et al. Facile method to enhance the adhesion of TiO_2 nanotube arrays to Ti substrate. *ACS Appl Mater Interfaces*. 2014;6:8001. doi:10.1021/am5015716
15. Wei W, Berger S, Hauser C, Meyer K, Yang M, Schmuki P. Transition of TiO_2 nanotubes to nanopores for electrolytes with very low water contents. *Electrochem Commun*. 2010;12:1184. doi:10.1016/j.elecom.2010.06.014
16. Jarosz M, Syrek K, Kapusta-Kołodziej J, et al. Heat treatment effect on crystalline structure and photoelectrochemical properties of anodic TiO_2 nanotube arrays formed in ethylene glycol and glycerol based electrolytes. *J Phys Chem C*. 2015;119:24182. doi:10.1021/acs.jpcc.5b08403
17. Rasouli MR, Restrepo C, Maltenfort MG, Purtill JJ, Parvizi J. Risk factors for surgical site infection following total joint arthroplasty. *J Bone Joint Surg Am*. 2014;96:e158. doi:10.2106/JBJS.M.00453
18. Deng C, Shen X, Yang W, et al. Construction of zinc-incorporated nano-network structures on a biomedical titanium surface to enhance bioactivity. *Appl Surf Sci*. 2018;453:263. doi:10.1016/j.apsusc.2018.05.097
19. Liu R, Tang Y, Zeng L, et al. *In vitro* and *in vivo* studies of anti-bacterial copper-bearing titanium alloy for dental application. *Dent Mater*. 2018;34:1112.
20. Mangram AJ, Horan TC, Pearson ML, Silver LC, Jarvis WR. Guideline for prevention of surgical site infection. *Am J Infect Control*. 1999;27:97. doi:10.1016/S0196-6553(99)70088-X
21. Pawlik A, Jarosz M, Syrek K, Sulka GD. Co-delivery of ibuprofen and gentamicin from nanoporous anodic titanium dioxide layers. *Colloids Surf B*. 2017;152:95. doi:10.1016/j.colsurfb.2017.01.011
22. Shen X, Zhang F, Li K, et al. Cecropin B loaded TiO_2 nanotubes coated with hyaluronidase sensitive multilayers for reducing bacterial adhesion. *Mater Design*. 2016;92:1007. doi:10.1016/j.matdes.2015.12.126
23. Wang G, Jin W, Qasim AM, et al. Antibacterial effects of titanium embedded with silver nanoparticles based on electron-transfer-induced reactive oxygen species. *Biomaterials*. 2017;124:25. doi:10.1016/j.biomaterials.2017.01.028
24. Kang SJ, Park SJ, Mishig-Ochir T, Lee BJ. Antimicrobial peptides: therapeutic potentials. *Expert Rev Anti-Infe*. 2014;12:1477. doi:10.1586/14787210.2014.976613
25. Alves D, Pereira MO. Mini-review: antimicrobial peptides and enzymes as promising candidates to functionalize biomaterial surfaces. *Biofouling*. 2014;30:483. doi:10.1080/08927014.2014.889120
26. Xhindoli D, Pacor S, Benincasa M, Scocchi M, Gennaro R, Tossi A. The human cathelicidin LL-37-a pore-forming antibacterial peptide and host-cell modulator. *Biochim Biophys Acta*. 2016;1858:546. doi:10.1016/j.bbamem.2015.11.003
27. Rajasekaran G, Kim EY, Shin SY. LL-37-derived membrane-active FK-13 analogs possessing cell selectivity, anti-biofilm activity and synergy with chloramphenicol and anti-inflammatory activity. *Biochim Biophys Acta*. 2017;1859:722. doi:10.1016/j.bbamem.2017.01.037
28. Coffelt SB, Marini FC, Watson K, et al. The proinflammatory peptide LL-37 promotes ovarian tumor progression through recruitment of multipotent mesenchymal stromal cells. *Proc Natl Acad Sci U S A*. 2009;106:3806. doi:10.1073/pnas.0900244106
29. He Y, Mu C, Shen X, et al. Peptide LL-37 coating on micro-structured titanium implants to facilitate bone formation *in vivo* via mesenchymal stem cell recruitment. *Acta Biomater*. 2018;80:412. doi:10.1016/j.actbio.2018.09.036
30. Popat KC, Eltgroth M, Latempa TJ, Grimes CA, Desai TA. Decreased staphylococcus epidermis adhesion and increased osteoblast functionality on antibiotic-loaded titania nanotubes. *Biomaterials*. 2007;28:4880. doi:10.1016/j.biomaterials.2007.07.037

31. Chau TT, Bruckard WJ, Koh PTL, Nguyen AV. A review of factors that affect contact angle and implications for flotation practice. *Adv Colloid Interface Sci*. 2009;150:106. doi:10.1016/j.cis.2009.07.003
32. Bhushan B, Jung YC. Wetting, adhesion and friction of superhydrophobic and hydrophilic leaves and fabricated micro/nanopatterned surfaces. *J Phys Condens Mat*. 2008;20:225010. doi:10.1088/0953-8984/20/22/225010
33. Wachem PBV, Beugeling T, Feijen J, Bantjes A, Detmers JP, Aken WGV. Interaction of cultured human endothelial cells with polymeric surfaces of different wettabilities. *Biomaterials*. 1985;6:403–408.
34. Park JH, Wasilewski CE, Almodovar N, et al. The responses to surface wettability gradients induced by chitosan nanofilms on micro-textured titanium mediated by specific integrin receptors. *Biomaterials*. 2012;33:7386. doi:10.1016/j.biomaterials.2012.06.066
35. Lee JH, Lee HB. A wettability gradient as a tool to study protein adsorption and cell adhesion on polymer surfaces. *J Biomat Sci Polym E*. 1993;4:15.
36. Brammer KS, Oh S, Cobb CJ, Bjursten LM, van der Heyde H, Jin S. Improved bone-forming functionality on diameter-controlled TiO_2 nanotube surface. *Acta Biomater*. 2009;5:3215. doi:10.1016/j.actbio.2009.04.029
37. Park J, Bauer S, von der Mark K, Schmuki P. Nanosize and vitality: TiO_2 nanotube diameter directs cell fate. *Nano Lett*. 2007;7:1686. doi:10.1021/nl070678d
38. Li M, Yang Y. Nanoscale TiO_2 nanotubes as a basis for governing cell behaviors and application challenges. *Int J Nanomed*. 2017;12:575. doi:10.2147/IJN.S128749
39. He Y, Zhang Y, Shen X, et al. The fabrication and in vitro properties of antibacterial polydopamine-LL-37-POPC coatings on micro-arc oxidized titanium. *Colloids Surf B*. 2018;70:54. doi:10.1016/j.colsurfb.2018.05.070
40. Losic D, Simovic S. Self-ordered nanopore and nanotube platforms for drug delivery applications. *Expert Opin Drug Deliv*. 2009;6:1363. doi:10.1517/17425240903300857
41. Zeth K, Sancho-Vaello E. The human antimicrobial peptides dermcidin and LL-37 show novel distinct pathways in membrane interactions. *Front Chem*. 2017;5:86. doi:10.3389/fchem.2017.00059
42. Henzler Wildman KA, Lee DK, Ramamoorthy A. Mechanism of lipid bilayer disruption by the human antimicrobial peptide, LL-37. *Biochemistry*. 2003;42:6545. doi:10.1021/bi0273563
43. Lozeau LD, Rolle MW, Camesano TA. A QCM-D study of the concentration-and time-dependent interactions of human LL37 with model mammalian lipid bilayers. *Colloids Surf B*. 2018;167:229. doi:10.1016/j.colsurfb.2018.04.016
44. Ahmed TAE, Hammami R. Recent insights into structure–function relationships of antimicrobial peptides. *J Food Biochem*. 2018;2018:e12546.
45. Yu X, Quan J, Long W, et al. LL-37 inhibits LPS-induced inflammation and stimulates the osteogenic differentiation of BMSCs via P2X7 receptor and MAPK signaling pathway. *Exp Cell Res*. 2018;372:178. doi:10.1016/j.yexcr.2018.09.024
46. Liu Z, Yuan X, Liu M, et al. Antimicrobial peptide combined with BMP2-modified mesenchymal stem cells promotes calvarial repair in an osteolytic model. *Mol Ther*. 2018;26:199. doi:10.1016/j.ymthe.2017.09.011